Hyperfine coupling of point defects in semiconductors by hybrid density functional calculations: The role of core spin polarization

Krisztián Szász,[1,2] Tamás Hornos,[1] Martijn Marsman,[3] and Adam Gali[1,4,*]

[1]*Institute for Solid State Physics and Optics, Wigner Research Centre for Physics, Hungarian Academy of Sciences, P.O. Box 49, H-1525 Budapest, Hungary*

[2]*Institute of Physics, Loránd Eötvös University, Pázmány Péter sétány 1/A, H-1117 Budapest, Hungary*

[3]*Computational Materials Physics, Faculty of Physics, University of Vienna, Sensengasse 8/12, 1090 Wien, Austria*

[4]*Department of Atomic Physics, Budapest University of Technology and Economics, Budafoki út 8, H-1111 Budapest, Hungary*

(Received 14 March 2013; revised manuscript received 19 June 2013; published 7 August 2013)

We implemented the calculation of hyperfine tensors into such plane wave supercell code working with the projector augmentation wave method that incorporates hybrid density functional theory and the contribution of the spin polarization of the core states. We show that the combination of HSE06 hybrid density functional together with the contribution of the core spin polarization provides accurate results on prominent point defects in various semiconductors, where the latter effect may be enormously large, in contrast to previous expectations. We briefly discuss the relevance of our results in the light of realization of solid-state quantum bits by paramagnetic point defects.

DOI: 10.1103/PhysRevB.88.075202 PACS number(s): 76.30.−v, 61.72.J−, 61.82.Fk, 71.15.Mb

I. INTRODUCTION

Hyperfine coupling is an interaction between the electronic and nuclear spin. This interaction, for instance, makes it possible to detect the presence of hydrogen molecules across the universe, by means of the famous 21 cm^{-1} line in the electron paramagnetic resonance (EPR) spectrum.[1,2] The hyperfine tensor ($A_{ij}^{(J)}$) between the electron spin density $\sigma(\mathbf{r})$ of electron spin S, and the nuclei (J) with nonzero nuclear spin (I) may be written as

$$A_{ij}^{(J)} = \frac{1}{2S}\gamma_J\gamma_e\hbar^2\left[\frac{8\pi}{3}\int \delta(\mathbf{r}-\mathbf{R}_J)\sigma(\mathbf{r})d\mathbf{r} + W_{ij}(\mathbf{R}_J)\right], \quad (1)$$

where the first term within the square brackets is the so-called (isotropic) Fermi-contact term, and

$$W_{ij}(\mathbf{R}) = \int\left(\frac{3(\mathbf{r}-\mathbf{R})_i(\mathbf{r}-\mathbf{R})_j}{|\mathbf{r}-\mathbf{R}|^5} - \frac{\delta_{ij}}{|\mathbf{r}-\mathbf{R}|^3}\right)\sigma(\mathbf{r})d\mathbf{r} \quad (2)$$

represents the (anisotropic) dipole-dipole contribution to the hyperfine tensor. γ_J is the nuclear Bohr magneton of nucleus J and γ_e the electron Bohr magneton. The Fermi-contact term is proportional to the magnitude of the electron spin density at the center of the nucleus which is equal to the trace of $\frac{1}{3}A^{(J)}$. The principal values of the $A^{(J)}$ tensor are the hyperfine constants that are often labeled as A_{xx}, A_{yy}, and A_{zz}.

By close inspection of Eqs. (1) and (2) one can realize that the chemical composition via γ_J and the spin density distribution of the investigated system may be determined by EPR and EPR-related spectroscopies. The spin density distribution is dominantly associated with the wave functions of the unpaired electrons. This makes the EPR-related spectroscopies a very powerful method to identify point defects in host semiconductors. Electrically or optically active point defects in semiconductors have often such charge states where their stable or long-living metastable spin state is paramagnetic ($S > 0$). In addition, either the impurity or the host semiconductor may contain $I > 0$ nuclei. Thus, hyperfine interaction between the electron spin and the nuclei spins may unravel the atom types constituting the defect. In addition, largest hyperfine coupling on these systems can identify to which atoms the spin density, and so the defect wave functions, are mostly localized. This makes it possible to set up microscopic models on EPR centers where comparison between experimental data and *ab initio* values on hyperfine tensors can significantly contribute to identification of point defects in semiconductors.[3–10]

Besides the identification of point defects, the hyperfine interaction has another great importance in defect physics. The hyperfine coupling in paramagnetic point defects in semiconductors is responsible for the entanglement between the electronic and nuclear spins. This interaction serves as a base to realize solid-state quantum bits from point defects.[11–16] A prominent example is the nitrogen-vacancy defect (NV) in diamond that operates at room temperature[11] and shows that hyperfine coupling between electron and nuclei spins can be very robust. Hyperfine coupling can be also used to map the electron spin into nuclear spin[17–20] with relatively long coherence time. Intricate details about the magnitude and direction of the hyperfine field created by these paramagnetic point defects should be known[21] in order to apply them for quantum computing[22,23] or remote sensing.[24–27] A reliable and relatively accurate method for calculating the hyperfine couplings is an immediate need in this hot topic.

To this end, we implemented the evaluation of hyperfine tensors into the plane wave, all-electron projector augmentation (PAW) code VASP[28,29] where we take the contribution of the core spin polarization to the Fermi-contact term into account with valence-frozen spin density approximation. Our new implementation allows us to calculate the hyperfine tensors of point defects in large supercells, convergent basis sets, and accurate HSE06[30,31] valence spin densities. We found on well-selected point defects in various group-IV semiconductors that only the combination of HSE06 functional and the contribution of the core spin polarization can consequently account for the experimental signals. We

show on the NV defect that in stark contrast to previous findings, the core spin polarization has a significant effect. We present evidence that the core contribution in the hyperfine coupling is giant in a promising candidate for realizing solid-state quantum bits,[16,32–34] the silicon vacancy in 4H SiC.

In order to present our achievements and results, we organized our paper as follows. We describe the implementation of hyperfine calculation in Sec. II. Then, we give the defect systems and the parameters applied to model the chosen point defects in Sec. III. The results are given and discussed in detail in Sec. IV. Finally, we conclude our paper in Sec. V.

II. IMPLEMENTATION OF THE HYPERFINE CALCULATION

Our implementation of the computation of hyperfine tensors closely follows the work of Blöchl.[35] Within the PAW framework,[29,36] the spin density σ can be written as

$$\sigma = \widetilde{\sigma} + \sigma^1 - \widetilde{\sigma}^1, \tag{3}$$

where $\widetilde{\sigma}$ is the pseudo-spin-density, and σ^1 and $\widetilde{\sigma}^1$ are one-center expansions of the true- and pseudo-spin-densities, respectively. In VASP, $\widetilde{\sigma}$ is expanded in plane waves, whereas the one-center terms are represented on radial logarithmic grids.

The plane wave contribution to the Fermi contact term is conveniently calculated from the pseudo-spin-density in reciprocal space, as

$$\widetilde{\sigma}(\mathbf{R}) = \sum_{\mathbf{G}} \widetilde{\sigma}(\mathbf{G}) e^{i\mathbf{G}\cdot\mathbf{R}}. \tag{4}$$

The one-center contributions are a bit more involved. These contributions can be written as a sum of the products of atom-centered radial functions and real spherical harmonics Y_L:

$$\sigma^1(\mathbf{r}) = \sum_{\mathbf{R}} \sum_{L} \sigma^1_{L\mathbf{R}}(|\mathbf{r}-\mathbf{R}|) Y_L(\widehat{\mathbf{r}-\mathbf{R}}). \tag{5}$$

The true spin density at atomic site $\mathbf{R}$ is then obtained from the s-like contribution in this expansion, through

$$\int \delta_T(r) \sigma^1_{s\mathbf{R}}(r) dr, \tag{6}$$

where the delta function of Eq. (1) has been replaced by a more extended function δ_T to account for relativistic effects. For details on δ_T and the way the integral of Eq. (6) is evaluated see Eqs. (A1) and (A6) in the Appendix of Ref. 35. The contributions of the pseudo one-center spin density $\widetilde{\sigma}^1$ to the Fermi contact terms is evaluated analogously.

From Eqs. (2) and (3) we have that the anisotropic contributions to the hyperfine tensors may be written as

$$W_{ij}(\mathbf{R}) = \widetilde{W}_{ij}(\mathbf{R}) + W^1_{ij}(\mathbf{R}) - \widetilde{W}^1_{ij}(\mathbf{R}), \tag{7}$$

where the contribution $\widetilde{W}_{ij}(\mathbf{R})$, coming from the pseudo-spin-density $\widetilde{\sigma}$, may again be conveniently evaluated in reciprocal space:

$$\widetilde{W}_{ij}(\mathbf{R}) = -4\pi \sum_{\mathbf{G}} \left(\frac{G_i G_j}{G^2} - \frac{\delta_{ij}}{3} \right) \widetilde{\sigma}(\mathbf{G}) e^{i\mathbf{G}\cdot\mathbf{R}}. \tag{8}$$

The one-center contributions to $W_{ij}(\mathbf{R})$ stem from d-like terms in the expansion of Eq. (5), and can written as

$$\begin{aligned}
W^1_{xx}(\mathbf{R}) &= \sqrt{\frac{12\pi}{5}} \left(-\frac{1}{\sqrt{3}} D^1_{3z^2-r^2,\mathbf{R}} + D^1_{x^2-y^2,\mathbf{R}} \right), \\
W^1_{yy}(\mathbf{R}) &= \sqrt{\frac{12\pi}{5}} \left(-\frac{1}{\sqrt{3}} D^1_{3z^2-r^2,\mathbf{R}} - D^1_{x^2-y^2,\mathbf{R}} \right), \\
W^1_{zz}(\mathbf{R}) &= \sqrt{\frac{12\pi}{5}} \sqrt{\frac{4}{3}} D^1_{3z^2-r^2,\mathbf{R}}, \quad W^1_{xy}(\mathbf{R}) = \sqrt{\frac{12\pi}{5}} D^1_{xy,\mathbf{R}}, \\
W^1_{xz}(\mathbf{R}) &= \sqrt{\frac{12\pi}{5}} D^1_{xz,\mathbf{R}}, \quad W^1_{yz}(\mathbf{R}) = \sqrt{\frac{12\pi}{5}} D^1_{yz,\mathbf{R}},
\end{aligned} \tag{9}$$

where

$$D^1_{L,\mathbf{R}} = \int_{0+}^{r_c} \frac{\sigma^1_{L\mathbf{R}}(r)}{r^3} dr \tag{10}$$

and r_c is the cutoff radius of the one-center expansions. Similarly, the pseudo-one-center contributions to the anisotropic part of the hyperfine tensor, $\widetilde{W}^1_{ij}(\mathbf{R})$, are found from the d-like terms in the real spherical harmonics expansion of $\widetilde{\sigma}^1$.

In VASP, as in most other implementations of the PAW method, the expansion of Eq. (3) involves the valence electronic spin density only. To estimate the contribution of the core electrons to the Fermi contact term we follow the approach of Yazyev *et al.*[37] and compute the spin polarization of the core electrons within the frozen valence approximation. In short, we solve the scalar-relativistic radial Schrödinger equation self-consistently for the core electronic states, keeping the spin-polarized valence density fixed. For these calculations, exchange and correlation were treated using the Perdew-Burke-Ernzerhof (PBE) functional.[38]

In order to verify that our implementation of the core contribution to the hyperfine tensor follows that of Yazyev *et al.*, we compare their results with ours on some organic molecules and radicals. We could not make a complete direct comparison since they utilized pseudopotential plane-wave density functional theory, and such general gradient approach for the exchange-correlation functional[39,40] that is not implemented in our code. The conclusion of their work is that the core spin polarization correction recovers the largest part of the error when compared to all-electron calculations and experimental results. They put the molecules in a $12 \times 12 \times 12$ Å^3 cubic box. The plane wave cutoff was 100 Ry (∼1360 eV). Our calculations were performed in $20 \times 20 \times 20$ Å^3 isolated cubic box at the Γ point. This size of the box was large enough to avoid the overlap of the wave functions in the periodic images. The kinetic energy cutoff was 500 eV, which was sufficient to obtain convergent hyperfine constants (or spin densities) within the PAW method. We optimized the geometry only with the PBE functional in this case. Concerning the hyperfine constants calculated by the HSE06 functional, the PBE-optimized geometries were applied.

The results are summarized in Table I. The values of the valence spin densities are similar which shows us that the use of the PBE functional is appropriate for comparison. The core polarization has similar order of magnitude in both calculations. For HCO and FCO molecules we get slightly different results. This is due to the large charge transfer among

TABLE I. The calculated Fermi-contact terms in MHz unit. The values of the PP PW column correspond to the pseudopotential plane wave approach, and the PP PW + CSPC column corresponds to the same method corrected for core spin polarization (from Ref. 37). PBE and HSE columns represent our obtained results with PBE and HSE06 functionals with or without the contribution of the core states (A_{1c}). In the parentheses the relative magnitude of the core contributions (CSPC and A_{1c}) are showed compared to the values without core corrections (PP PW and PBE without A_{1c}), respectively.

system	isotope	PP PW[a]	PP PW + CSPC[a]	PBE without A_{1c}[b]	PBE with A_{1c}[b]	HSE without A_{1c}[b]	HSE with A_{1c}[b]	experiment[c]
CH_3	^{1}H	−65.3		−64.2		−72.0		−64.6
	^{13}C	186.1	74.3(60.1)	182.5	86.1(52.8)	198.1	101.9	107.4
C_2H_3	^{1}H	43.7		44.1		35.7		35.9
	^{1}H	181.9		182.7		177.8		184.7
	^{1}H	113.9		114.7		111.5		111.0
	^{13}C	−23.3	−11.5(50.6)	−20.1	−10.9(45.9)	−34.8	−21.5	−24.1
	^{13}C	395.1	297.1(24.8)	377.4	292.6(22.5)	407.3	318.5	301.5
H_2CN	^{1}H	238.8		240.0		230.4		233.2
	^{13}C	−75.4	−61.9(17.8)	−70.6	−59.3(16.0)	−90.6	−74.6	−81.0
	^{14}N	59.1	11.8(80.1)	58.7	15.0(74.5)	70.4	24.1	26.1
HCO	^{1}H	375.0		369.2		373.5		379.5
	^{13}C	454.0	411.1(9.4)	414.8	376.5(9.2)	429.0	389.0	375.3
	^{17}O	−64.5	−26.6(58.7)	−60.2	−18.9(68.5)	−73.8	−32.3	−42.3
FCO	^{19}F	1136.4	972.2(14.5)	1040.1	844.4(18.8)	1027.0	824.8	905.8
	^{13}C	851.7	822.8(3.4)	800.2	773.4(3.3)	828.4	799.1	803.2
	^{17}O	−71.5	−46.5(34.9)	−65.1	−36.7(43.7)	−70.3	−42.7	
NO_2	^{14}N	174.0	160.6(7.7)	163.0	149.1(8.5)	164.3	148.4	153.6
	^{17}O	−91.9	−51.8(43.6)	−84.9	−42.2(50.4)	−87.5	−43.4	−45.7 to -56.9

[a]From Ref. 37.
[b]Present work.
[c]From Ref. 41–50.

the atoms, which can depend on the choice of the functional. All in all, we could fairly reproduce Yazyev *et al.*'s results related to the core correction. We mention that for these molecules the core contribution can be large (even ∼50%) concerning the carbon isotope. Furthermore, the HSE06 functional provides surprisingly good results on hyperfine couplings when compared to the experimental values.

Having this new tool in our hand, we use this implementation on defects with deep levels where these defects induce molecular-like states embedded in a crystalline matrix.

III. DEFECT SYSTEMS AND MODELING

We first study the prominent negatively charged nitrogen-vacancy defect (NV center) in diamond. Next, we investigate the negatively charged silicon vacancy (V_{Si}) in 4*H* SiC. V_{Si} is a basic defect and a leading candidate to realize solid-state quantum bits in 4*H* SiC.[16,32–34] Nevertheless, the hyperfine interactions in V_{Si} are far from being understood. We briefly mention that two inequivalent substitutional sites exist in 4*H* SiC that we label by *h* and *k* sites. Correspondingly, $V_{Si}(h)$ and $V_{Si}(k)$ are studied in detail. Finally, we study such deep-level defects in Si that were first found by EPR techniques:[51] A center[52,53] and E center.[54] These centers have well-established microscopic origin: strongly reconstructed substitutional oxygen (also called VO center) and phosphorus-vacancy complex (PV), respectively. These defects are excellent test beds for our methodology.

We use 512-atom simple cubic supercells for Si and diamond and a 576-atom supercell for 4*H* SiC. Sampling of the first Brillouin zone is often limited to the Γ point, which generally suffices for these large supercells. However, 2×2×2 Monkhorst-Pack sets of *k* points[55] are also applied when the calculated defect levels are close to the band edges of the host semiconductor. The plane wave basis set cuts off at a kinetic energy of 420 eV, which is sufficiently convergent for the hyperfine constants in the considered systems.[56] Both semilocal PBE and the hybrid HSE06 functionals are applied to calculate the hyperfine tensors of the defect. First, we optimized the lattice constants for each functional, and we carried out geometry optimization (criteria of forces: 0.01 eV/Å). The calculated band gaps of Si, diamond, and 4*H* SiC are 1.12 (0.52), 5.4 (4.2), and 3.16 (2.20) eV by HSE06 (PBE), respectively (compared to the experimental values of 1.17, 5.45, and 3.23 eV, respectively). We note that the conduction band minimum of these systems folds onto the Γ point of the supercells. Previous HSE06 results imply that not just the electronic structure of the host semiconductor is improved by HSE06 functional[57] but also the defect states are well described in them,[58] so it is expected that the spin density is also well described that it is the important quantity to obtain accurate hyperfine interaction.

IV. RESULTS AND DISCUSSION

We wish to focus our attention on the role of the core contribution thus we discuss the results from this point of view. Also, we deal with the band gap problem where it is needed. The key results are summarized in Table II. Next, we discuss each defect system in detail.

TABLE II. Relative percentage errors of the calculated hyperfine constants compared to the experimental values. For the sake of simplicity, in each system we consider only those $I > 0$ isotopes which have the largest hyperfine constants. These atoms are labeled in the isotope column, and in the figures of each systems (Figs. 1–4), as well. In order to compare the calculated with the experimental hyperfine values readily, the average of the principal values of the hyperfine tensor $[(A_{xx} + A_{yy} + A_{zz})/3]$ is taken for both the calculated and the experimental results. [The individual principal values can be found in the Supplemental Material (Ref. 56): NV: Tables XXI and XXII, V_{Si}: Tables XXIII–XXVI, VO: Tables XVII and XVIII, PV: Tables XIX and XX.] The absolute errors are also shown in the parentheses in MHz unit. PBE and HSE columns represent the obtained results with PBE and HSE06 functionals with or without the contribution of the core states (A_{1c}). MAE is mean average error, and MSE is square root of mean-squared error of the shown data. In the case of VO and PV defects 2×2×2 Monkhorst-Pack k-point scheme was used with PBE functional otherwise Γ point was applied (see text for details).

system	isotope	PBE without A_{1c}	PBE with A_{1c}	HSE without A_{1c}	HSE with A_{1c}
NV[a]	$^{13}C_{1-3}$	0.32(0.41)	21.04(29.11)	18.27(25.83)	3.77(4.70)
$V_{Si}(k)$[b]	$^{13}C_{2-4}$	20.87(8.87)	22.72(9.12)	47.69(20.38)	2.03(1.49)
$V_{Si}(h)$[b]	$^{13}C_{2-4}$	21.34(9.54)	23.37(9.18)	46.75(20.64)	5.11(2.73)
VO[c]	$^{29}Si_{1,2}$	15.23(62.22)	14.68(59.99)	1.62 (6.42)	0.93(3.62)
PV[d]	$^{29}Si_1$	15.63(53.01)	16.07(54.48)	10.84(34.09)	11.46(36.14)
MAE		14.67	19.58	25.03	4.66
MSE		18.57	22.58	35.10	7.09

[a]Experimental data are taken from Ref. 59.
[b]Experimental data are taken from Ref. 60.
[c]Experimental data are taken from Ref. 52 and 53.
[d]Experimental data are taken from Ref. 54.

A. NV center in diamond

The negatively charged NV defect is a prominent color center in diamond which has become a leading solid-state quantum-measurement tool. In the NV defect the nitrogen substitutes one carbon atom adjacent a nearby vacancy. The symmetry is C_{3v} where a double-degenerate e defect state in the gap is occupied by two electrons with parallel spins ($S = 1$).[59,61–63] The spin density is mostly localized on the nearest-neighbor ^{13}C atoms of the vacancy (see Fig. 1) where the corresponding hyperfine couplings were already investigated in great detail by (semi)local functionals.[21,63,64] Our PBE results are in good agreement with earlier work,[21,64] obtained with a different plane wave PAW code.[65] These results

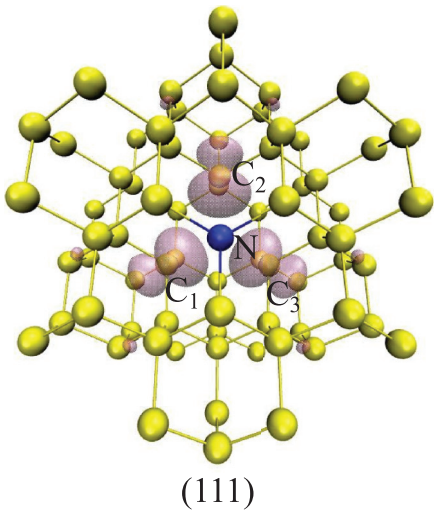

FIG. 1. (Color online) The isosurface of the calculated spin density for NV center (isovalue: 0.0560 1/Å^3) shown from (111) plane. The carbon (nitrogen) atoms are yellow (blue) balls. We obtain considerable spin density on the labeled carbon atoms, so these ^{13}C isotopes have significant hyperfine couplings.

are in a surprisingly good agreement with experiment when the spin density is calculated solely from the valence states (see Table II and Table XXI in the Supplemental Material[56]). Thus, previous findings implied that this solid-state quantum bit is fully understood. Our HSE06 calculations combined with core spin polarization unravel that PBE valence spin densities are too delocalized. Due to the presence of the nonlocal Fock-exchange in the HSE06 functional, HSE06 tends to localize the defect states. As a consequence, the largest hyperfine constants on the nearest-neighbor ^{13}C atoms become larger than the experimental value when only valence states are considered. However, we found that the spin polarization of the core state on ^{13}C atoms is very significant and accounts for about 20% of the Fermi-contact interaction. The spin polarization of the 1s orbitals compensates the spin polarization from the valence electrons; thus the absolute value of the hyperfine constants reduces. As a consequence, the HSE06 value *together with the contribution of the core spin polarization* is very close to the experimental data. Our study reveals that the calculated PBE hyperfine constants only from valence states just fortuitously agree well with the experimental data: The underestimation of the localization of the defect wave functions and the neglect of the spin polarization of the core electrons compensate each other.

We mention that we calculated the hyperfine tensor for PBE-optimized geometry with HSE functional and vice versa, in order to separate the effect of the geometry produced by the different functionals after geometry optimization and the spin density distributions at a given geometry produced by different functionals. The difference among the hyperfine values was within 2–3 % when different geometry but the same functional were applied. The core polarization has significantly larger contribution to the change in the hyperfine tensor elements (∼20%) than what the change in the geometry due to different functionals would imply. We conclude that the localization of the spin density has the major role in the calculated hyperfine

tensors when different functionals are applied, and not the slight change in the geometry induced by these functionals. Our finding highlights the significance of core contribution to the Fermi-contact hyperfine coupling that we demonstrate in our next example.

B. $V_{Si}(h,k)$ in 4*H* SiC

For the negatively charged V_{Si} in 4*H* SiC, it is of high importance to explore the hyperfine couplings of these centers in great detail;[16,32–34] however, the experimental and theoretical data on this center are scarce. The two possible configurations [Fig. 2(a) and Fig. 2(b)] have not been unambiguously assigned to the detected EPR centers associated with V_{Si} in 4*H* SiC. The spin density is mostly localized on the four C dangling bonds [Fig. 2(a) and Fig. 2(b)] that creates an e and a_1 level in the gap with C_{3v} symmetry. These levels are occupied by three electrons with parallel spins ($S = 3/2$).[32] We find that both PBE and HSE06 calculations predict larger hyperfine constants for the nearest-neighbor ^{13}C atoms at h site than those at k site. By that way we can conclusively identify Si-vacancy (I) and Si-vacancy (II) EPR signals[60] with k and h sites which goes opposite to the interpretation by Mizuochi and co-workers.[60] We note that the effect of the spin density of core states can be severe as found for the NV center in diamond. Interestingly, the PBE without core contribution yields too high (∼20%) while that with core contribution too low (∼20%) hyperfine constants compared to experimental data. This shows that PBE spin density cannot yield accurate hyperfine interaction for this basic defect in 4*H* SiC.

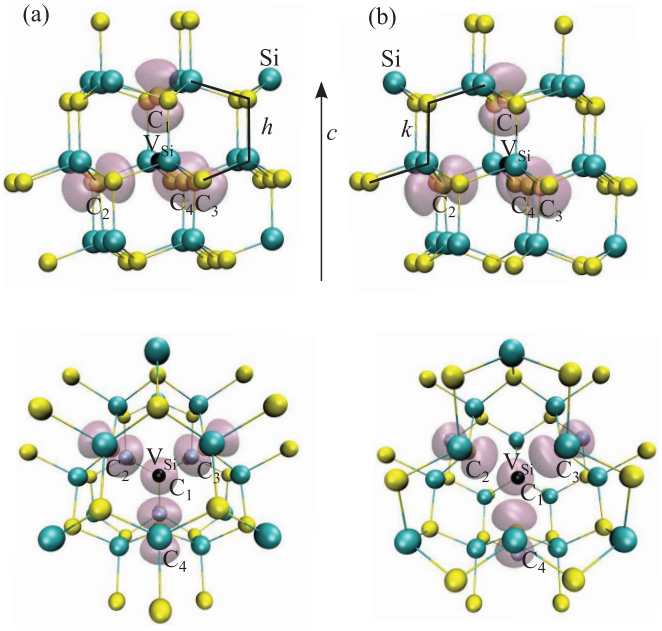

FIG. 2. (Color online) The isosurface of the calculated spin density (isovalue: 0.0600 1/Å^3) for V_{Si} defects at h (a) and k (b) site. Top panel: side view, bottom panel: top view. The silicon (carbon) atoms are blue (yellow) balls, while the missing silicon atom is depicted by a small black ball. ^{13}C isotopes with largest hyperfine couplings are labeled. The arrow with c shows the [0001] direction (c axis) of the hexagonal SiC lattice. The hexagonal (h) and quasicubic (k) sequence of Si-C bilayers are indicated by thick lines in the top panel.

HSE06 again localizes the defect states. This localization of the valence states and the corresponding spin density, however, would bring the hyperfine constants about 47% off from the experimental data. Including the spin polarization of the core states together with HSE06 functional can only reproduce the experimental data within a good accuracy because of the large contribution of the core spin polarization. This is an important finding with showing the physics of the system: (i) The HSE06 functional should be indeed an accurate functional to describe the valence electrons of V_{Si} in 4*H* SiC, and (ii) the hyperfine tensor of V_{Si} can be well reproduced by the HSE06 functional when the contribution of the core spin polarization to the Fermi-contact term is taken into account. This contribution is giant and reaches ∼40%.

In addition, we found that the spin density decays very fast from the center of silicon vacancies. Thus, the coherence time of the V_{Si} qubits may not be limited very much due to the presence of proximate ^{29}Si or ^{13}C nuclei. We found proximate 12 ^{29}Si and 20 ^{13}C atoms at h site while 8 ^{29}Si and 21 ^{13}C atoms at k site with hyperfine constants larger than 1 MHz where their $I = 1/2$ spin can be entangled to $S = 3/2$ spin by hyperfine interaction.[56] Further experimental studies motivated by our findings may support our identification of V_{Si} at inequivalent sites.

C. VO center in silicon

We now study the hyperfine signals of known microscopic origin where the spin density is not localized on light isotopes such as ^{13}C. The first deep-level defects discovered by EPR techniques in Si are such test bed examples. The VO center is a common defect in Si.[52] Substitutional oxygen strongly reconstructs along the [100] axis and binds to two nearest-neighbor oxygen atoms, leaving two Si dangling bonds behind. Its symmetry is C_{2v}. The A center[52] is a negatively charged VO defect ($S = 1/2$) where the unpaired electron occupies the antibonding b_1 orbital in the gap, that is strongly localized on the Si dangling bonds. The Γ-only PBE calculations underestimate the hyperfine constants on the $Si_{1,2}$ atoms in Fig. 3 by roughly 50% compared to experimental data (see Tables I and IV in the Supplemental Material[56]). This artificial delocalization is due to the band gap error of the PBE functional. The b_1 level lies very close to the conduction

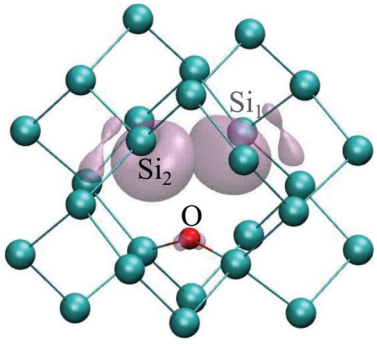

FIG. 3. (Color online) The isosurface of the calculated spin density of A center in silicon. The chosen isosurface value is 0.02. The substitutional oxygen atom is clouded by the lobes of spin density which is dominantly localized on two Si atoms labeled as Si_1 and Si_2.

band minimum (CBM) and hybridizes strongly with these band states. Using MP 2×2×2 k-point sampling the CBM is not sampled in the supercell calculation, thus reducing this hybridization. As a consequence, the PBE 2×2×2 results show a great improvement compared to those of PBE Γ but the discrepancy is still ≈15% (Table II). The HSE06 Γ calculations are in almost perfect agreement with experiment, for $^{29}Si_{1,2}$ isotopes (Table II). The occupied b_1 level lies 0.36 eV below the CBM in this case. We also note that hyperfine couplings with other approximate ^{29}Si isotopes were detected that can be also well-reproduced by HSE06.[56]

D. PV center in silicon

The PV defect is common in P-doped electron-irradiated Si.[54] The neutral PV defect has $S = 1/2$ and yields the E center in the EPR spetrum. The PV defect consists of a P atom substituting one Si atom in the lattice near a vacancy. The defect has an axial C_{3v} symmetry along the [111] direction and creates one fully occupied a_1 level and a singly occupied e level in the gap. The e state is localized on the Si-dangling bonds of the vacancy while the a_1 state is partially localized on the P atom. This system is Jahn-Teller unstable due to the partial occupation of the orbitally degenerate state; thus the system should reconstruct to C_{1h} symmetry. The $C_{3v} \rightarrow C_{1h}$ distortion splits the e state, $e \rightarrow a' \oplus a''$, and $a_1 \rightarrow a'$. This allows a mixing between a' orbitals in C_{1h} symmetry; thus the unpaired electron can "borrow" the character of the original a_1. Consequently, a small hyperfine coupling on the ^{31}P isotope is expected. Two configurations of C_{1h} distortion is feasible (Fig. 4): *conf1* with a short-base triangle [Fig. 4(a)] and *conf2* with a long-base triangle [Fig. 4(b)] of Si atoms around the vacancy. The spin density is localized on one (two) Si dangling bonds in *conf1* (*conf2*) configurations. In the low-temperature EPR measurements *conf1* was measured as large hyperfine signal was detected on a single ^{29}Si,[54] and it should be the stable configuration. However, PBE Γ calculation predicts *conf2* configuration as stable which contradicts the experimental finding. Again, this error is due to the band gap problem of the PBE functional. The highest occupied a' defect level lies close to CBM and mixes with it resulting in false geometry and spin density distribution. PBE 2×2×2 calculation predicts the appropriate geometry, and the spin density distribution qualitatively follows the experiment. However, the absolute value of the largest hyperfine constant on ^{29}Si is still about 16% smaller than the experimental one because the defect state is too delocalized (see Ref. 56). The HSE06 functional correctly provided the *conf1* geometry as the most stable configuration, and it localizes the defect state due to the non-local Fock exchange. As a consequence, HSE06 Γ calculation yields relatively good agreement for the largest hyperfine coupling. All in all, HSE06 can significantly improve the results compared to those obtained by PBE.

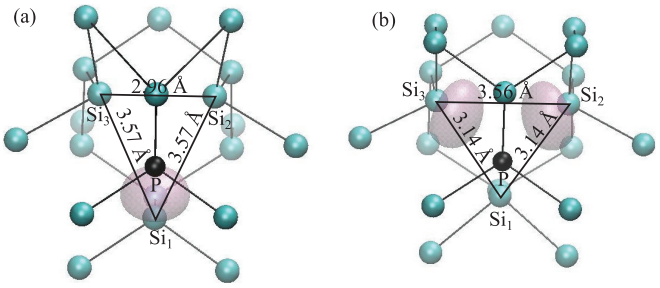

FIG. 4. (Color online) Two two possible C_{1h} distortions of PV defect in Si. P atom is shown as black ball. The isosurface of calculated spin densities and distances are depicted as obtained by HSE06 method. (a) *conf1*, (b) *conf2* configuration. *conf1* is more stable than *conf2*.

V. CONCLUSION

In summary, we implemented the calculation of hyperfine tensors within a plane wave supercell PAW framework where the HSE06 valence spin density can be combined with the contribution of the core spin polarization. By applying our method on prominent point defects in semiconductors we found that, principally, only the combination of the two describes the physics of the system. The contribution of the core spin polarization may be giant as demonstrated in silicon vacancies in 4H SiC.

ACKNOWLEDGMENT

Support from EU FP7 project DIAMANT (Grant No. 270197) is acknowledged.

*agali@eik.bme.hu

[1] H. I. Ewan and E. M. Purcell, Nature (London) **168**, 356 (1951).
[2] C. A. Muller and J. H. Oort, Nature (London) **168**, 357 (1951).
[3] H. Overhof, M. Scheffler, and C. M. Weinert, Phys. Rev. B **43**, 12494 (1991).
[4] C. G. Van de Walle and P. E. Blöchl, Phys. Rev. B **47**, 4244 (1993).
[5] A. Gali, P. Deák, N. Son, E. Janzén, H. von Bardeleben, and J.-L. Monge, Mater. Sci. Forum **433-436**, 511 (2003).
[6] M. Bockstedte, M. Heid, and O. Pankratov, Phys. Rev. B **67**, 193102 (2003).
[7] H. Overhof and U. Gerstmann, Phys. Rev. Lett. **92**, 087602 (2004).
[8] T. Umeda, N. T. Son, J. Isoya, E. Janzén, T. Ohshima, N. Morishita, H. Itoh, A. Gali, and M. Bockstedte, Phys. Rev. Lett. **96**, 145501 (2006).
[9] N. T. Son, P. Carlsson, J. ul Hassan, E. Janzén, T. Umeda, J. Isoya, A. Gali, M. Bockstedte, N. Morishita, T. Ohshima, and H. Itoh, Phys. Rev. Lett. **96**, 055501 (2006).
[10] U. Gerstmann, Phys. Status Solidi B **248**, 1319 (2011).
[11] L. Childress, M. V. Gurudev Dutt, J. M. Taylor, A. S. Zibrov, F. Jelezko, J. Wrachtrup, P. R. Hemmer, and M. D. Lukin, Science **314**, 281 (2006).
[12] J. J. L. Morton, A. M. Tyryshkin, R. M. Brown, S. Shankar, B. W. Lovett, A. Ardavan, T. Schenkel, E. E. Haller, J. W. Ager, and S. A. Lyon, Nature (London) **455**, 1085 (2008).
[13] C. B. Simmons, J. R. Prance, B. J. Van Bael, T. S. Koh, Z. Shi, D. E. Savage, M. G. Lagally, R. Joynt, M. Friesen, S. N. Coppersmith, and M. A. Eriksson, Phys. Rev. Lett. **106**, 156804 (2011).

[14]G. W. Morley, P. Lueders, M. H. Mohammady, S. J. Balian, G. Aeppli, C. W. M. Kay, W. M. Witzel, G. Jeschke, and T. S. Monteiro, Nat. Mat. **12**, 103 (2013).
[15]W. F. Koehl, B. B. Buckley, F. J. Heremans, G. Calusine, and D. Awschalom, Nature (London) **479**, 84 (2011).
[16]D. Riedel, F. Fuchs, H. Kraus, S. Väth, A. Sperlich, V. Dyakonov, A. A. Soltamova, P. G. Baranov, V. A. Ilyin, and G. V. Astakhov, Phys. Rev. Lett. **109**, 226402 (2012).
[17]G. D. Fuchs, V. V. Dobrovitski, R. Hanson, A. Batra, C. D. Weis, T. Schenkel, and D. D. Awschalom, Phys. Rev. Lett. **101**, 117601 (2008).
[18]B. Smeltzer, J. McIntyre, and L. Childress, Phys. Rev. A **80**, 050302 (2009).
[19]V. Jacques, P. Neumann, J. Beck, M. Markham, D. Twitchen, J. Meijer, F. Kaiser, G. Balasubramanian, F. Jelezko, and J. Wrachtrup, Phys. Rev. Lett. **102**, 057403 (2009).
[20]G. D. Fuchs, V. V. Dobrovitski, D. M. Toyli, F. J. Heremans, C. D. Weis, T. Schenkel, and D. D. Awschalom, Nat. Phys. **6**, 668 (2010).
[21]B. Smeltzer, L. Childress, and A. Gali, New J. Phys. **13**, 025021 (2011).
[22]M. V. Gurudev Dutt, L. Childress, L. Jiang, E. Togan, J. Maze, F. Jelezko, A. S. Zibrov, P. R. Hemmer, and M. Lukin, Science **316**, 1312 (2007).
[23]P. Neumann, N. Mizuochi, F. Rempp, P. Hemmer, H. Watanabe, S. Yamasaki, V. Jacques, T. Gaebel, F. Jelezko, and J. Wrachtrup, Science **320**, 1326 (2008).
[24]A. Dréau, J.-R. Maze, M. Lesik, J.-F. Roch, and V. Jacques, Phys. Rev. B **85**, 134107 (2012).
[25]S. Kolkowitz, Q. P. Unterreithmeier, S. D. Bennett, and M. D. Lukin, Phys. Rev. Lett. **109**, 137601 (2012).
[26]T. H. Taminiau, J. J. T. Wagenaar, T. van der Sar, F. Jelezko, V. V. Dobrovitski, and R. Hanson, Phys. Rev. Lett. **109**, 137602 (2012).
[27]N. Zhao, J. Honert, B. Schmid, M. Klas, J. Isoya, M. Markham, D. Twitchen, F. Jelezko, R.-B. Liu, H. Fedder, and J. Wrachtrup, Nat. Nanotechnol. **7**, 657 (2012).
[28]G. Kresse and J. Furthmüller, Phys. Rev. B **54**, 11169 (1996).
[29]G. Kresse and D. Joubert, Phys. Rev. B **59**, 1758 (1999).
[30]J. Heyd, G. E. Scuseria, and M. Ernzerhof, J. Chem. Phys. **118**, 8207 (2003).
[31]A. V. Krukau, O. A. Vydrov, A. F. Izmaylov, and G. E. Scuseria, J. Chem. Phys. **125**, 224106 (2006).
[32]A. Gali, J. Mat. Res. **27**, 897 (2012).
[33]V. A. Soltamov, A. A. Soltamova, P. G. Baranov, and I. I. Proskuryakov, Phys. Rev. Lett. **108**, 226402 (2012).
[34]P. G. Baranov, V. A. Soltamov, A. A. Soltamova, G. V. Astakhov, and V. V. Dyakonov, Mater. Sci. Forum **740–742**, 425 (2012).
[35]P. E. Blöchl, Phys. Rev. B **62**, 6158 (2000).
[36]P. E. Blöchl, Phys. Rev. B **50**, 17953 (1994).
[37]O. V. Yazyev, I. Tavernelli, L. Helm, and U. Röthlisberger, Phys. Rev. B **71**, 115110 (2005).
[38]J. P. Perdew, K. Burke, and M. Ernzerhof, Phys. Rev. Lett. **77**, 3865 (1996).
[39]A. D. Becke, Phys. Rev. A **38**, 3098 (1988).
[40]J. P. Perdew, Phys. Rev. B **33**, 8822 (1986).
[41]D. M. Chipman, Theor. Chim. Acta **82**, 93 (1992).
[42]E. Hirota and C. Yanada, J. Mol. Spectrosc. **96**, 175 (1985).
[43]R. W. Fessenden and R. H. Schuler, J. Chem. Phys. **39**, 2147 (1963).
[44]R. W. Fessenden, J. Phys. Chem. **71**, 74 (1967).
[45]H. J. McManus, R. W. Fessenden, and D. M. Chipman, J. Phys. Chem. **92**, 3778 (1988).
[46]H. J. McManus, R. W. Fessenden, and D. M. Chipman, J. Phys. Chem. **92**, 3781 (1988).
[47]F. J. Adrian, B. F. Kim, and J. Bohandy, J. Chem. Phys. **82**, 1804 (1985).
[48]F. J. Adrian, E. L. Cochran, and V. A. Bowers, J. Chem. Phys. **43**, 462 (1965).
[49]E. L. Cochran, F. J. Adrian, and V. A. Bowers, J. Chem. Phys. **44**, 4626 (1966).
[50]Z. Luz, A. Reuveni, R. W. Holmberg, and B. L. Silver, J. Chem. Phys. **51**, 4017 (1969).
[51]G. Feher, Phys. Rev. **114**, 1219 (1959).
[52]G. D. Watkins and J. W. Corbett, Phys. Rev. **121**, 1001 (1961).
[53]R. van Kemp, M. Sprenger, E. G. Sieverts, and C. A. J. Ammerlaan, Phys. Rev. B **40**, 4054 (1989).
[54]G. D. Watkins and J. W. Corbett, Phys. Rev. **134**, A1359 (1964).
[55]H. J. Monkhorst and J. K. Pack, Phys. Rev. B **13**, 5188 (1976).
[56]See Supplemental Material at http://link.aps.org/supplemental/10.1103/PhysRevB.88.075202 for additional data about the methods and hyperfine constants of defects.
[57]M. Marsman, J. Paier, A. Stroppa, and G. Kresse, J. Phys.: Condens. Matter **20**, 064201 (2008).
[58]P. Deák, B. Aradi, T. Frauenheim, E. Janzén, and A. Gali, Phys. Rev. B **81**, 153203 (2010).
[59]S. Felton, A. M. Edmonds, M. E. Newton, P. M. Martineau, D. Fisher, D. J. Twitchen, and J. M. Baker, Phys. Rev. B **79**, 075203 (2009).
[60]N. Mizuochi, S. Yamasaki, H. Takizawa, N. Morishita, T. Ohshima, H. Itoh, and J. Isoya, Phys. Rev. B **68**, 165206 (2003).
[61]J. H. N. Loubser and J. A. van Wyk, Rep. Prog. Phys. **41**, 1201 (1978).
[62]J. P. Goss, R. Jones, S. J. Breuer, P. R. Briddon, and S. Öberg, Phys. Rev. Lett. **77**, 3041 (1996).
[63]A. Gali, M. Fyta, and E. Kaxiras, Phys. Rev. B **77**, 155206 (2008).
[64]A. Gali, Phys. Rev. B **80**, 241204 (2009).
[65]P. E. Blöchl, C. J. Först, and J. Schimpl, Bull. Mater. Sci. **26**, 33 (2003).